Composites Part B 219 (2021) 108963

Contents lists available at ScienceDirect

Composites Part B

journal homepage: www.elsevier.com/locate/compositesb

Layered double hydroxide/graphene oxide synergistically enhanced polyimide aerogels for thermal insulation and fire-retardancy

Tiantian Xue [a], Wei Fan [a,**], Xiang Zhang [a], Xingyu Zhao [a], Fan Yang [a], Tianxi Liu [a,b,*]

[a] State Key Laboratory for Modification of Chemical Fibers and Polymer Materials, College of Materials Science and Engineering, Innovation Center for Textile Science and Technology, Donghua University, 2999 North Renmin Road, Shanghai, 201620, PR China

[b] Key Laboratory of Synthetic and Biological Colloids, Ministry of Education, School of Chemical and Material Engineering, Jiangnan University, Wuxi, 214122, PR China

ARTICLE INFO

Keywords:
A. polyimide aerogel
A. LDH-GO hybrids
B. thermal insulation
B. fire-retardancy

ABSTRACT

Environmentally friendly materials with lightweight, good thermal insulation and fire-resistance are highly required for energy efficient buildings. Here, layered double hydroxide (LDH) - graphene oxide (GO) synergistically enhanced polyimide (PI) aerogels with great thermal insulation, good thermal stability and excellent flame retardancy, have been designed and synthesized through a green environmental freeze-drying method followed by thermal imidization. LDH can be uniformly dispersed in aqueous solutions by electrostatic interactions with GO, thus resulting in uniform dispersion in PI matrix. Due to the physical interaction between the two kinds of nanosheets and PI, the pore size of PI/LDH-GO (PLG) composite aerogel was significantly reduced from 20 μm to 5 μm, leading to ultralow density (52 ± 3.6 mg cm^{-3}), low thermal conductivity (36 ± 1.7 mW m^{-1} K^{-1}), and high compressive modulus (26 ± 1.8 MPa). More importantly, the addition of two pollution-free fire-retardants (LDH-GO) endows the PLG aerogels excellent fire-resistant performance with the limiting oxygen index reach up to 43 ± 1.2%, reaching the nonflammable level. Therefore, this work paves a new way for anti-flaming and heat insulating materials with great potential for practical applications in energy efficient buildings.

1. Introduction

Accounting for about 40% of the world's energy consumption is used to create a comfortable indoor environment [1,2]. Improving energy efficiency is critical to the sustainable development of society. At present, the installation of thermal insulation materials in buildings is a widely adopted solution [3,4]. However, the commercial polymer-based insulation materials such as polyurethane (PU) and expanded polystyrene (PS) of are limited by their poor thermal stability, high thermal conductivity and flammability (limited oxygen index, LOI<27%) due to their intrinsic molecular structure [5–8]. Pursuing low density and low thermal conductivity is of great significance for excellent building insulating materials. More significantly, the frequent fires highlight the importance of flame-retardant and high-temperature resistant building insulating materials.

Aerogel is defined as a gel comprised of a microporous solid in which the dispersed phase is gas [9]. Due to its unique three-dimensional porous structure, the aerogel exhibits low apparent density, high specific surface area, high porosity and extremely low thermal conductivity, which makes aerogel the first choice for energy efficient building materials [10]. Although silica aerogels have undergone in-depth research, their wide application is still restricted due to the problems of brittleness, poor mechanical strength, easy powdering, and time-consuming and costly preparation process [11,12]. In comparison to silica aerogels, polymer aerogels with designable molecular structure, excellent mechanical properties, and low energy consumption have attracted wide attentions [13,14]. However, the widely researched polymer aerogels such as poly (vinyl alcohol) (PVA), cellulose, and chitosan face the problems of poor thermal stability, easily degradation and flammability, which limits their application in the field of energy efficient buildings [15–17]. To minimize the flammability of those polymer aerogels, various types of flame retardants, for example hydroxyapatite (HAP), graphene oxide (GO), silicon dioxide (SiO_2), and inorganic layered compounds have been successfully compounded with polymer aerogels

* Corresponding author. State Key Laboratory for Modification of Chemical Fibers and Polymer Materials, College of Materials Science and Engineering, Innovation Center for Textile Science and Technology, Donghua University, 2999 North Renmin Road, Shanghai, 201620, PR China.
** Corresponding author.
E-mail addresses: weifan@dhu.edu.cn (W. Fan), txliu@fudan.edu.cn, txliu@dhu.edu.cn (T. Liu).

https://doi.org/10.1016/j.compositesb.2021.108963
Received 27 February 2021; Received in revised form 17 April 2021; Accepted 4 May 2021
Available online 7 May 2021

[18–20]. For example, Wang et al. reported a unidirectional freeze-casing technique to assemble graphene-confined zirconium phosphate (ZrP/RGO) nanosheets with cellulose nanofibers (CNF) to prepare ZrP/RGO/CNF aerogel, which exhibits thermal conductivity of 18 mW m^{-1} K^{-1} and LOI of 33.5% [21]. However, the compression strength cannot meet the requirements of energy efficient building materials, and moreover, ZrP will release toxic gases during combustion. Zhu et al. fabricated composite aerogel based on a combination of HAP and chitosan, exhibiting excellent fire resistance [22]. However, the excellent flame retardancy requires the addition of a large amount of HAP (20 wt%-200 wt%), which dramatically increases the density of the composite aerogel. Therefore, polymer-based composite aerogels with low density, high strength, as well as fire-retardancy and thermal insulation are highly desirable for practical applications in building insulation.

Recently, polyimide (PI) aerogel has attracted wide attentions due to its excellent mechanical properties, wide operating temperature, good corrosion and radiation resistance and self-extinguishing properties [23]. For instance, Wang et al. reported a multifunctional PI aerogel textile obtained by a freeze-spinning technique, with excellent fire-retardant and temperature-resistant performance [24]. Furthermore, Wang et al. fabricated a robust and fire-retarded PI/MXene aerogels via freeze-drying and thermal imidization, exhibiting the peak heat release rate of 49.8 W g^{-1} [25]. Liu et al. prepared PI/GO composites by in-situ polymerization of PI on GO. During the combustion process, GO will accumulate and cover the PI surface to form a protective layer. These graphite layers will effectively increase the LOI value by preventing the transfer of oxygen and heat [26]. However, a large amount of smoke will be generated during the combustion process of PI, which may cause suffocation of personnel at the fire site. Therefore, further improving the fire resistance and smoke suppressing performance of PI aerogels is of great importance. Layered double hydroxide (LDH) is a non-toxic, smoke suppressing and environmentally friendly flame retardant, which has been widely applied as additives for flame-retardant polymer composites [27]. However, there are strong interaction between the host layer and the interlayer anion of LDH, which hinders the dispersion of LDH in solvents and polymer matrix. Therefore, it is still a challenge to achieve uniform dispersion of LDH in the polymer matrix, thereby improving the overall performance of the polymer aerogel.

In this work, LDH-GO synergistically reinforced PI composite aerogels have been reported with robust mechanical behavior, high fire retardancy and excellent thermal insulation performance. The PI/LDH-GO (PLG) composite aerogels were synthesized by a pollution-free freeze-drying method and thermal imidization process. Because of the large number of hydrophilic groups, GO can stabilize LDH nanosheets in aqueous solution by electrostatic interaction, thus leading to homogenous distribution of LDH-GO hybrids in PI matrix. The resulting PLG aerogels display the integrated performance of low density (52 ± 3.6 mg cm^{-3}), high porosity (>93%), and high compression modulus (26 ± 1.8 MPa). More importantly, due to the synergetic interaction of two inorganic nanosheets, the PLG aerogels exhibit super-insulation and high flame-retardant performance, which shows broad application prospects in energy efficient buildings and other fields.

2. Material and methods

The LDH-GO hybrids were obtained by a certain amount of LDH was added to the GO solution, further ultrasonicated (see details in supporting information). The LDH, GO and poly (amic acid) (PAA, polyimide precursor) was fabricated by according to previous works [23,28,29]. Briefly, PAA was dissolved in DI water, followed by adding LDH-GO hybrid solution, resulting in a homogenous PAA/LDH-GO hydrogel. The PLG aerogels were obtained by freeze-drying and thermal imidization. PLG aerogels incorporated with X wt% LDH and Y wt% GO were noted as PLG-XY. For comparison, binary composite aerogels with 6 wt% GO were noted as PG-6, and 6 wt% LDH were noted as PL-6, respectively.

3. Results and discussions

Fig. 1a illustrates the fabrication process for PLG aerogels. First, the as-prepared LDH (+) and GO (−) were homogenized in DI water to form well-dispersed LDH-GO hybrids. Afterwards, PAA solution were blended with above LDH-GO hybrids to form a homogeneous gel. After subsequent freeze-drying and thermal imidization, the PLG aerogel was finally obtained. During the thermal imidization process, GO is partially reduced as indicated by the Raman spectra (Fig. S1). As shown by the Raman spectra of PAA/LDH-GO and PLG aerogel in Fig. S1, the D/G band ratio of PLG (0.89) is higher than that of PAA/LDH-GO (0.70), indicating the enhanced graphitization of GO by thermal imidization [30]. The as-fabricated PLG aerogel can stand on the “setaria viridis” without any bending (Fig. 1b) due to its high porosity (>93%) and low density (low to 52 ± 3.6 mg cm^{-3}). In spite of its lightweight nature, the PLG aerogel is strong enough and exhibits good anti-compression properties. As shown in Fig. 1c and 0.4 g PLG aerogel can support a beaker containing 2000 ml of water without deformation, which is more than 5000 times its own weight. Furthermore, the PLG aerogels show good structural formability and can be tailored into letters of PI-LDH-GO (Fig. 1d). From infrared thermal images, the upper surface temperature of corresponding aerogels in the shape of letters (thickness of 5 mm) is under 100 °C with stage temperature above 200 °C, indicating the excellent thermal insulating ability of PLG aerogels.

The homogeneous dispersion of LDH-GO hybrids is the key premise for fabrication of PLG aerogels. SEM observations indicated that the LDH produced by urea-assisted co-precipitation exhibits a regular hexagonal shape, with size ranging from 1 to 2 μm and thickness of several tens of nanometers (Fig. 2a–c). The micro-size of LDH facilitates its embedding into the pore walls of aerogels. The XRD patterns of CO_3-LDH and NO_3-LDH are shown in Fig. S2. According to the XRD data, the interlayer distance of CO_3-LDH is 0.75 nm, and that of NO_3-LDH is increased to 0.83 nm, which is beneficial for the dispersion of LDH in water [31]. Fig. 2d shows the digital photographs of the GO, LDH-GO, and LDH aqueous suspension. Pure LDH can not be stably dispersed in water and precipitated at the bottom of the bottle. Interestingly, the LDH-GO hybrids with the mass ratio of 1:1 maintains stable dispersion (Fig. 2d), which is attributed to the remaining negative charge of GO and its hydrophilicity [32]. When the mass ratio of GO to LDH is 1:2 and 1:4, precipitation of LDH-GO occurs since the negative charge of GO is neutralized by the positive charge of LDH. This is further confirmed by zeta potential of GO, LDH-GO hybrids and LDH in aqueous solution (Fig. 2e). As shown in Fig. 2e, GO is negatively charged (−37.4 mV) while LDH is positively charged (+17.3 mV), indicating that GO is much more stable than LDH in aqueous solution. The zeta potential of LDH-GO hydribs is slightly less negative than that of GO, owing to the introduction of positively charged LDH. The zeta potential of LDH-GO hybrids with mass ratio of 1:1, 1:2 and 1:4 reaches −22.7 mV, −14.2 mV and −13.4 mV, respectively, indicating that LDH-GO hybrid at a mass ratio of 1:1 is more stable in aqueous solution than the two others. Hence, unless specifically stated, the PLG composite aerogels were prepared with LDH-GO hybrid at a mass ratio of 1:1. The uniformity of LDH in GO solution can be intuitively observed from TEM images (Fig. S3 & Fig. 2f), which clearly reveals that several LDH is scattered and tightly attached to GO, with wrinkles on the GO sheets that may caused by electrostatic adsorption between LDH (+) and GO (−). The successful synthesis of LDH-GO hybrid is also verified by the XRD characterization in Fig. S4, showing both the characteristic peaks of GO and LDH. In contrast, LDH is usually in a state of aggregation without GO (Fig. S5). SEM (Fig. 2g) and EDS mapping (Fig. 2h) images of PLG aerogel confirm the uniform distribution of LDH in the PI matrix, with the Mg and Al elements representing LDH uniformly distributed [33]. In addition, the hexagonal LDH sheets can be observed in the pore walls of PLG aerogel as shown by TEM images in Fig. S6, further indicating the

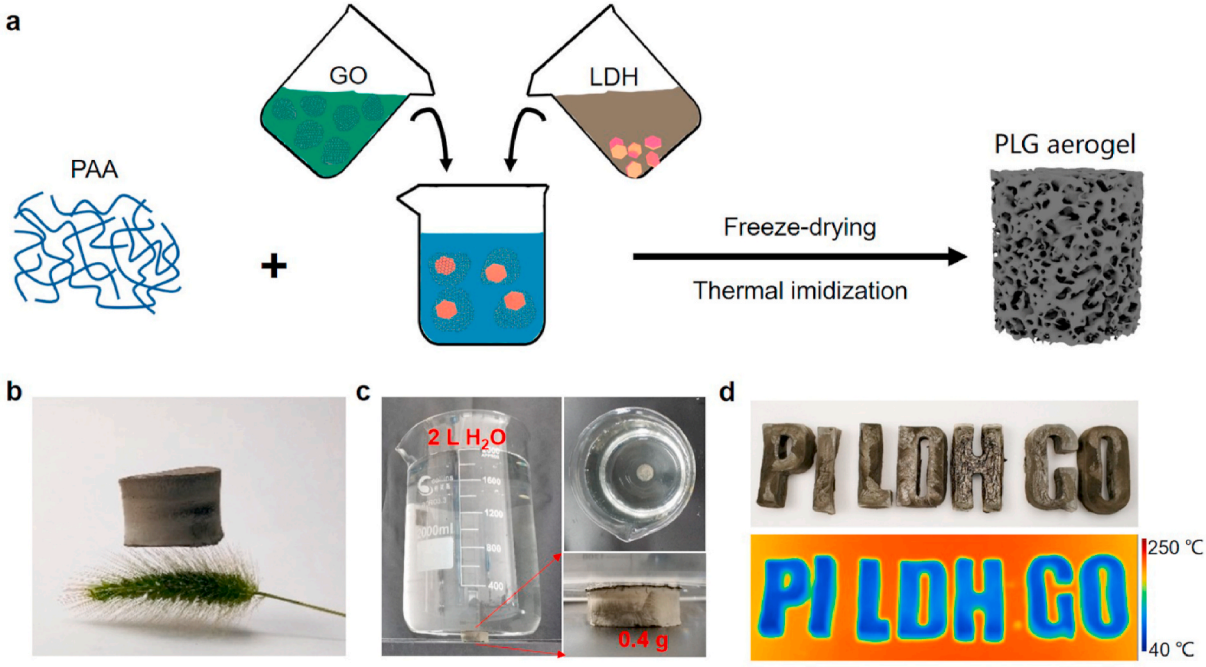

Fig. 1. Fabrication and characterization of the PLG aerogels. (a) Schematic illustration of the preparation of PLG aerogels. Digital photographs showing the PLG aerogels (b) standing on the "setaria viridis", (c) compressed by a beaker (2000 ml) with full water, and (d) that can be shaped into letters of PI-LDH-GO and corresponding infrared images of PLG aerogel on a 200 °C hot stage for 10 min.

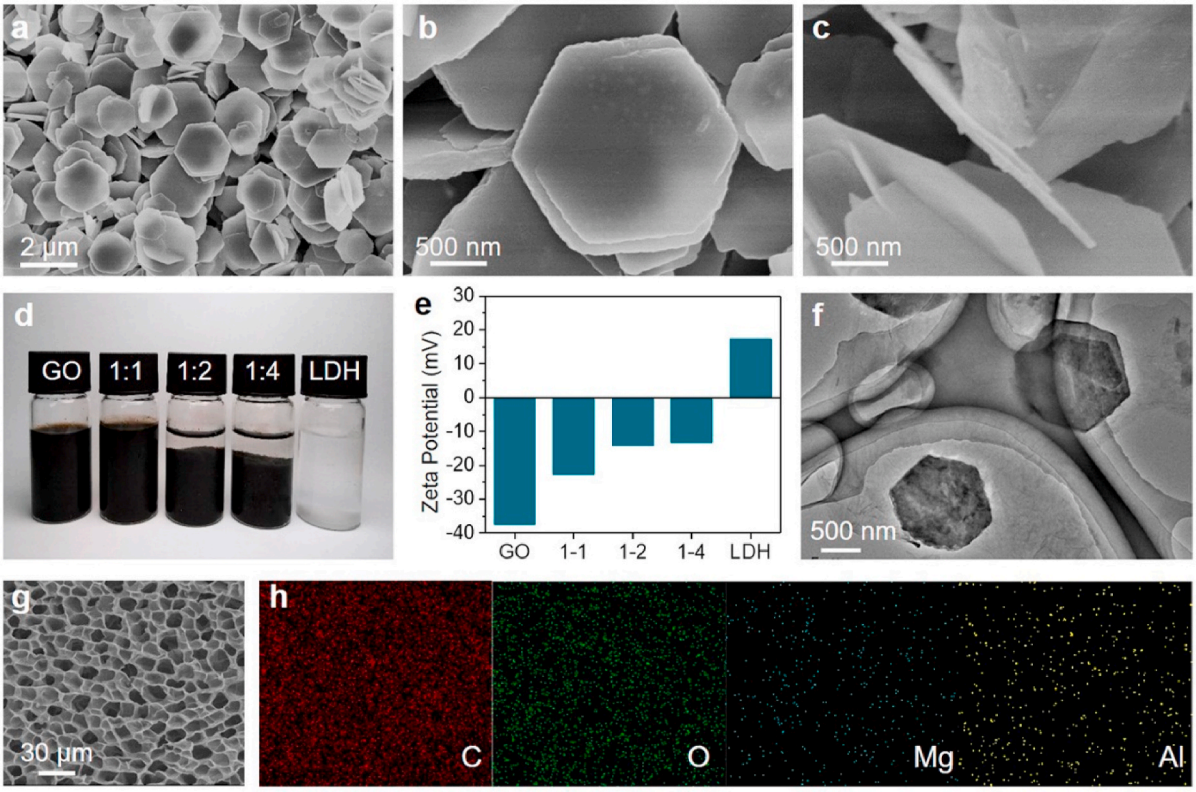

Fig. 2. Dispersity of LDH-GO hybrids. (a–c) SEM images of LDH. (d) Digital photographs of GO, LDH-GO, and LDH aqueous suspension. (e) Zeta potential of GO, LDH-GO and LDH in water. (f) TEM image of LDH-GO hybrids. (g) SEM images and (h) corresponding EDS mappings of C, O, Mg and Al of the PLG aerogel.

uniform distribution of LDH in the composite aerogel.

The typical SEM images of PI and PLG aerogels with varied LDH and GO contents are shown in Fig. 3. Typically, freeze-drying leads to an open porous structure with the pore size in the micron range. PI aerogel exhibited three-dimensional network with wrinkle pore walls and irregular pore size distribution (Fig. 3a and b). As for pure PI aerogel, it

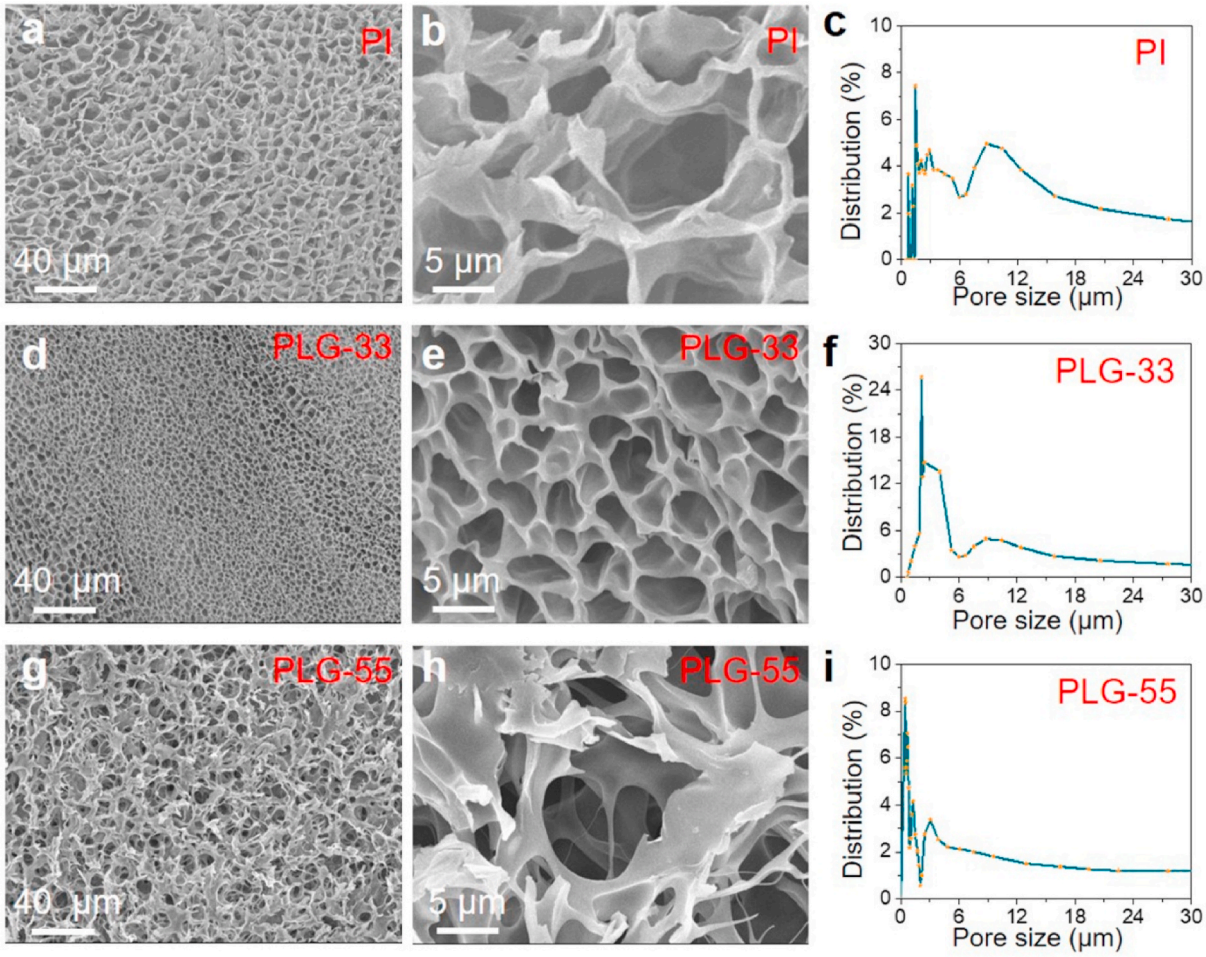

Fig. 3. Morphology of PI and PLG aerogels. SEM images of (a–b) PI aerogels, (d–e) PLG-33 aerogels, (g–h) PLG-55 aerogels, and (c, f, i) corresponding pore size distribution of the aerogels.

suffers from severe shrinkage during the freeze-drying and thermal imidization process, resulting in wrinkle pore walls. PI aerogel shows large pore size in the range of 3–20 μm with a broad distribution (Fig. 3c). However, the PLG-33 aerogel with incorporation of 3 wt% LDH and 3 wt% GO exhibited uniform three-dimensional network with smooth pore walls and pore size of ~5 μm (Fig. 3d and e). It can be clearly seen that the pore diameter of PLG-33 becomes smaller as compared with pure PI aerogel from the pore size distribution in Fig. 3f. The smaller pore size and smooth pore walls of PLG-33 aerogel are attributed to the strong physical or chemical interactions between PAA chain and GO during the gelation process, which could inhibit the shrinkage during the freeze-drying and thermal imidization [34]. As shown in Fig. S7a, the CO–NH bond of PAA/LDH-GO has a red shift due to the hydrogen bond between the GO sheets and PAA. Furthermore, the rheological behaviors of PAA/LDH-GO solution displayed a distinct shear-thinning behavior and a higher viscosity than that of PAA (Fig. S7b), also demonstrating a strong interaction existed between PAA chains and GO sheets [35]. However, with the excessive addition of LDH and GO, the connection of the PLG-55 aerogel pore wall became broken and even appeared fibrous structure, which can be presumably attributed to a large number of LDH-GO hybrids hindered the cross-linking of PAA during the sol-gel process (Fig. 3g and h). As for the pore size distribution (Fig. 3i), PLG-55 aerogel has a large number of small pores distributed, but in fact it is the fragmentation of large pore structure. The smaller pore size and continuous three-dimension porous structure of PLG-33 aerogel benefit the prolong of the heat conduction path, reducing the thermal conductivity and resisting the flame [36].

Thermal conductivity is an important index to evaluate the thermal insulation ability of energy building materials. As for PI aerogel, it suffers from severe shrinkage during the thermal imidization process, causing high density (85 ± 2.2 mg cm^{-3}), high shrinkage (47 ± 2.7%), low porosity (93.2 ± 1.8%), and high thermal conductivity (56 ± 1.2 mW m^{-1} K^{-1}) (Fig. 4a & Fig. S8). Interestingly, by simply integrating LDH-GO hybrids with PI, the PLG aerogel exhibits low density, low shrinkage, high porosity, and low thermal conductivity (Fig. 4a & Fig. S8). With the increase of LDH-GO content, the shrinkage rate of PLG aerogels is decreased from 47% to 29% with 3 wt% LDH and 3 wt% GO. This can be attributed to the fact that LDH-GO increases the cross-linking point which can support aerogel structure and share the thermal stress during the thermal imidization process. Meanwhile, the porosity also increases from 93% for PI to 96% for PLG-33 (Fig. S8b). Due to high porosity and low shrinkage, the density also decrease from 85 ± 2.2 mg cm^{-3} for PI to 52 ± 3.6 mg cm^{-3} for PLG-33 (Fig. S8c). Further increasing the content of LDH-GO, the shrinkage rate of PLG composite aerogels increases, resulting in reduced porosity and increased density, since the excess LDH-GO hybrids may aggregate and hinder the gelation of PAA. The PLG-33 aerogel with 3 wt% LDH and 3 wt% GO can achieve the lowest thermal conductivity of 36 ± 1.7 mW m^{-1} K^{-1}, much lower than that 56 ± 1.2 mW m^{-1} K^{-1} for pure PI aerogel, 49 ± 2.1 mW m^{-1} K^{-1} for PG-6 with 6 wt% GO, and 47 ± 1.4 mW m^{-1} K^{-1} for PL-6 with 6 wt% LDH (Fig. 4a). In contrast to pure PI aerogel without nanosheets, PLG-33 aerogels, benefiting from small pore size (5 μm) and appropriate amount of interfacial thermal resistance generated by nanosheets, the so-called Kapitza resistance, leading to both low solid thermal

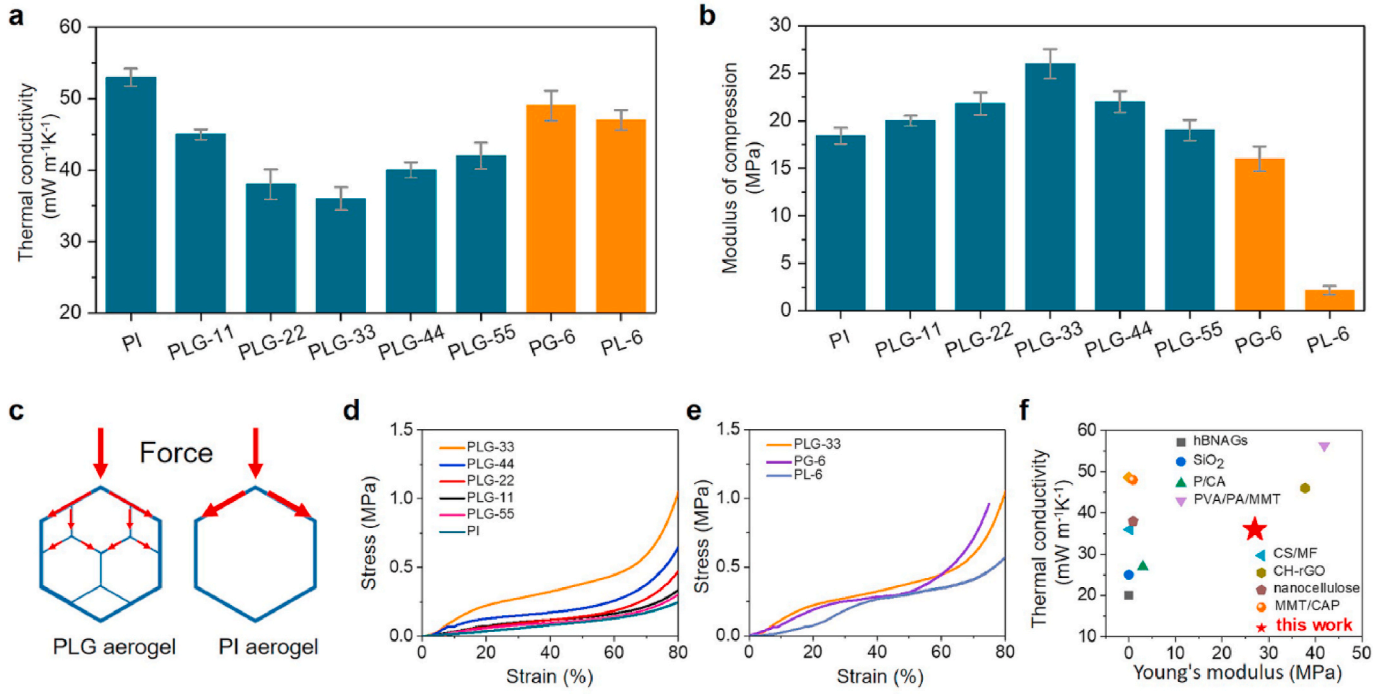

Fig. 4. Thermal insulation and mechanical properties of PLG aerogels. (a–b) Thermal conductivity and compression modulus of PI, PLG, PL, and PG aerogels. (c) The possible compression mechanisms of PLG and PI aerogels. (d, e) Strain-stress curves of PI, PLG, PL, and PG aerogels. (f) Thermal conductivity versus compression modulus for aerogel-like materials, including boron nitride aerogels (hBNAGs, Ref. [39]), SiO_2 aerogels (Ref. [40]), PVA/chitosan aerogels (P/CA, Ref. [41]), GO aerogels (Ref. [42]), nanocellulose aerogels (Ref. [43]), PVA/MMT (Ref. [44]), CS/MMT (Ref. [45]), MMT/CAP (Ref. [46]) and PLG aerogels.

conductivity and gas thermal conductivity [37]. The oxygen-rich functional groups of GO can form physical crosslinks with PAA, increase the degree of crosslinking, and reduce shrinkage and the density of aerogels, leading to improved thermal insulation properties of aerogels. Furthermore, in contrast to PG or PL with single nanosheet, PLG-33 aerogels, benefiting from multiple interfacial thermal resistance between PI, LDH and GO, exhibits reduced solid conduction of the wall, leading to low thermal conductivity. In addition, as shown in Fig. S9, the PLG-33 aerogels show similar thermal conductivity in different directions, indicating the isotropic feature of PLG-33 aerogels. Therefore, the PLG-33 composite aerogels with outstanding thermal insulation performance exhibit great potential for practical applications in energy efficient building.

Excellent mechanical strength is a prerequisite for practical application of aerogel materials. The compression modulus of PLG aerogels first increased and then decreased with the increase of LDH-GO nanosheets. Compared to 18 ± 1.1 MPa of PI aerogel, the compression modulus of PLG-33 aerogels reaches 26 ± 1.8 MPa (Fig. 4b). The high compression modulus of PLG-33 aerogel is mainly due to: (i) compared to large pores, smaller pores provide more paths to distribute stress (Fig. 4c), (ii) LDH-GO hybrids are evenly distributed in the pore wall of PLG-33 aerogel, which can further disperse the stress [4]. In contrast, the compression modulus of the PG-6 and PL-6 aerogels with the same amount of single nanosheets decreased, especially that PL-6 aerogel with 6 wt% LDH even decreased to 2.2 ± 0.5 MPa. This is due to that LDH is easy to aggregate and precipitate in the PI matrix, forming many stress concentration points, which are easily damaged when subjected to force. The corresponding stress-strain curves shown in Fig. 4d and e, typically exhibit three characteristic stages for honeycomd-like aerogels: a linear elastic regime at 0%–10% strain due to elastic deformation and slightly deformed pore structure, a subsequent plateau stage at 10%–60% strain because the pore structure begins to collapse, and finally a densification region after 60% strain since the overall plastic deformation occurs, leading to rapidly increased apparent density and stress [38]. Moreover, we compared the Young's modulus and the thermal conductivity of PLG aerogel with other typical fire-risistant aerogels (Fig. 4f). The PLG aerogel exhibits much higher Young's modulus than other aerogels listed in Fig. 4f with little difference in thermal conductivity [39–46], showing great potential for practical applications.

In order to further explore the flame retardancy of aerogels, we conducted cone calorimetry tests on PI aerogels and PLG-33 aerogels respectively, and corresponding heat release rate (HRR), total heat release (THR), total smoke release (TSR) and CO production (COP) were obtained (Fig. 5a–d and Table S1). The HRR curves revealed that PI aerogel burnt rapidly after ignited, and a sharp HRR peak (69.6 ± 1.1 kW m^{-2}) arose at 26 s (Fig. 5a). When 3 wt% LDH and 3 wt% GO were added, the HRR peak value (25.8 ± 1.0 kW m^{-2}) of the PLG-33 aerogel decreased by 63.7%, and the combustion time decreased by 61.8%, indicating that the addition of LDH-GO hybrids slowed down the combustion of PI aerogel. From the THR curves (Fig. 5b), the THR increase of PLG-33 aerogel was relatively slow, which is only 27% of that of PI aerogel in the end. Compared with the PI aerogel, the low HRR and THR of PLG-33 aerogel can be attributed to the formation of a shielding layer by LDH-GO hybrids to protect the underlying materials. The LDH-GO hybrid as a shielding layer can prevent the transfer of flammable small molecules generated by thermal degradation to the combustion interface, while delaying the diffusion of external O_2 into the interior [47]. The TSR is also significantly reduced with the addition of LDH-GO hybrids (Fig. 5c), probably because LDH can release water and CO_2 from hydroxides when been heated, thus reducing the concentration of combustible gas and blocking oxygen [48]. Although the increase rate of COP of PLG-33 aerogel is slightly higher than that of PI aerogel, the total COP is still very low, within a safe and acceptable range (Fig. 5d). In general, aerogels with higher limiting oxygen index (LOI) exhibit higher flame retardant ability [49]. Compared with PI aerogel, the LOI value of PG-6 aerogel, PL-6 aerogel and PLG-33 aerogel raise to 40 ± 1.3%, 42 ± 1.1% and 43 ± 1.2%, displaying that combustion condition for PLG-33 aerogel is the most demanding (Fig. 5e). TGA results show that the addition of LDH-GO also improves the thermal stability of aerogels (Fig. 5f). The main weight loss of the PI aerogel starts at 500 °C, while

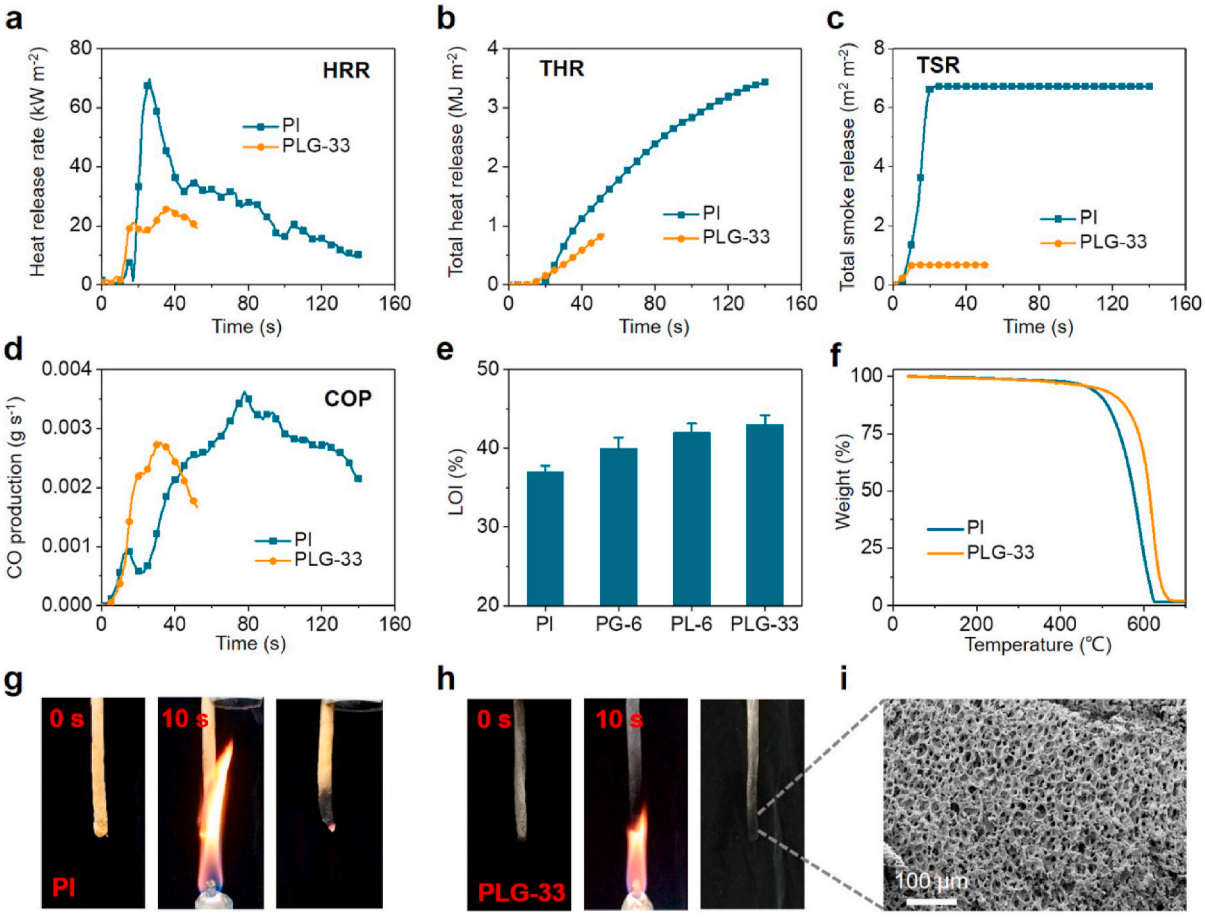

Fig. 5. Flame retardant and thermal stability of PLG aerogels. (a–d) Combustion behaviors of PLG-33 and PI aerogels by cone calorimeter test. (e) The LOI values of aerogels. (f) TGA curves of PLG-33 and PI aerogels under N_2 atmosphere. (g) Digital photographs of vertical combustion of pure PI aerogels in 10 s. (h) Digital photographs of vertical combustion of PLG-33 aerogels and (i) SEM image of corresponding PLG-33 aerogel after combustion.

the PLG-33 aerogel is delayed to 550 °C, which is much higher than the decomposition temperature of other polymer aerogels. During the thermal degradation of PLG-33 aerogel, LDH reacts with polymer to form a dense carbon layer, which can delay the thermal degradation rate of PI, leading to the increase of initial thermal decomposition temperature of PLG-33 as compared with PI aerogel [50]. After being soaked in ethanol and ignited, the volume of PI aerogel contracted seriously after full combustion, while PLG-33 aerogel self-extinguished after the consumption of ethanol, with the volume remained basically unchanged (Fig. S10). Through vertical combustion test, the pure PI aerogel burns violently and exhibits large shrinkage after burning (Fig. 5g). In contrast, PLG-33 aerogel has excellent self-extinguishing ability in the air, and basically does not produce smoke (Fig. 5h). The morphology of PLG-33 aerogel after vertical combustion (SEM image in Fig. 5i) indicates that the porous structure of PLG-33 aerogel remains, while the pore walls become thicker due to partial carbonization, which also explains the retention of the macroscopic morphology of aerogel. Therefore, it can be concluded that the addition of an appropriate amount of LDH-GO can inhibit the combustion and smoke release of the aerogel, and greatly improve the flame retardancy of the composite aerogel. The excellent flame retardancy of PLG aerogel improves its safety as a building insulating material.

It is necessary to study the thermal insulation behavior of thermal insulation materials at different temperatures for applications in wide temperature range. The thermal conductivity of PLG-33 aerogel rises slowly with increasing temperature from −50 °C to 300 °C (Fig. 6a). At −50 °C, its thermal conductivity is as low as 27 ± 1.3 mW m^{-1} K^{-1}, and with the temperature rises to 300 °C, the thermal conductivity is also lower than 65 ± 1.4 mW m^{-1} K^{-1}, which shows that PLG-33 aerogels are suitable for thermal insulation in different temperature environments. The low thermal conductivity makes the PLG-33 aerogels have potentiality of infrared stealth. In the infrared thermal image, the color of the PLG-33 aerogel with a thickness of 10 mm on the hand is almost the same as that of the environment, which means the covered part of the hand is invisible under infrared detection device (Fig. 6b). These excellent thermal insulation properties keep the upper surface temperature of the PLG-33 aerogel (thickness 10 mm) below 150 °C on the top of the flame for a long time (Fig. 6c). The thermal conductivity of PLG aerogel at 30 °C in humid environment was also investigated (Fig. S11). The PLG aerogel displays low thermal conductivities of 36 ± 1.7, 42 ± 1.0, 48 ± 1.4, 52 ± 2.0 and 57 ± 1.8 mW m^{-1} K^{-1} at 20%, 40%, 60% and 80% relative humidity, respectively (Fig. S11a). Although the thermal conductivity of PLG-33 aerogel increases with humidity slightly, it still remains quite a low level due to its hydrophobicity (Fig. S11b). Excellent fire resistance and thermal insulation are the most desirable properties of building cladding materials, especially for high-rise buildings. As a demonstration, we use PLG-33 aerogel (thickness of 5 mm) as the thermal insulation inner layer of a plastic “house”, and simulate the temperature change inside and outside the house using infrared light as the heat source (Fig. 6d). As shown in Fig. 6e, after 20 min of illumination, the external temperature (T_1) of the house has risen from 21 °C to 46 °C, and the internal temperature of the house (T_2) can still be maintained at a comfortable temperature below 30 °C to achieve human body thermal comfort [51] with the PLG-33 aerogel as thermal insulating layer. In comparison, the internal temperature rose rapidly and exceeded 36.3 °C after 20 min for “house” with commercial PS foam as

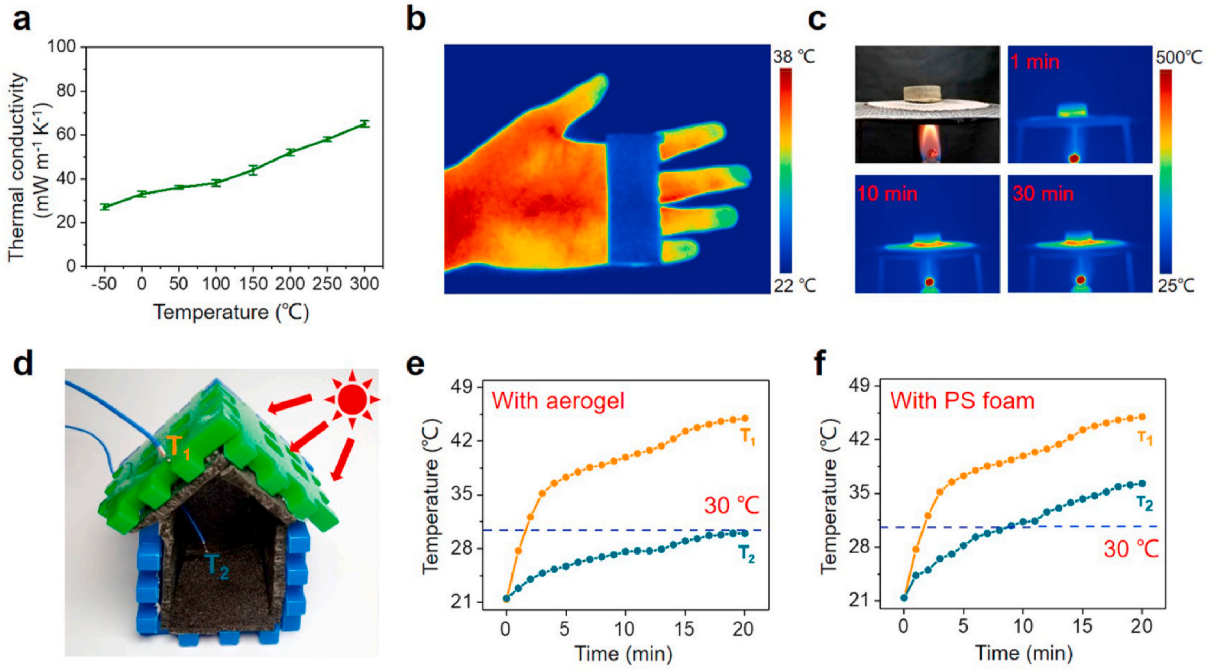

Fig. 6. Thermal insulating applications of PLG-33 aerogels. (a) Thermal conductivities of PLG-33 aerogel from −50 °C to 300 °C. (b) Thermal infrared images of PLG-33 aerogel placed on the hand. (c) Digital photograph and thermal infrared images of PLG-33 aerogel placed on a spirit lamp. (d) The photo of the small "house" using PLG-33 aerogel as thermal insulating inner layer. Temperature change with irradiation time by an infrared light (e) with PLG-33 aerogel and (f) with PS foam as inner layer.

interlayer (Fig. 6f & Fig. S12). This distinct difference indicates a favorable thermal insulating ability of the PLG-33 aerogel, demonstrating its great potential in the energy efficient buildings.

4. Conclusions

In conclusion, we report a newly designed polymer composite aerogel with high flame retardant, low thermal conductivity and high strength for thermal insulation applications. The PLG aerogel has been fabricated with the addition of LDH-GO hybrids, followed by freeze-drying and thermal imidization process. In the composites, GO improves the dispersion of LDH in PI matrix by electrostatic adsorption and excellent hydrophilic ability, thus improving the mechanical performance of PLG composite aerogel with high compression modulus up to 26 ± 1.8 MPa. Moreover, due to the reduced pore size caused by increased number of cross-linking points formed by GO and PI chains, the thermal conductivity of PLG-33 composite aerogel is reduced to 36 ± 1.7 mW m^{-1} K^{-1} at room temperature (27 ± 1.3 mW m^{-1} K^{-1} at −50 °C and 65 ± 1.4 mW m^{-1} K^{-1} at 300 °C). In addition, incorporation of LDH-GO hybrids can significantly enhance the flame retardancy of PI matrix, resulting in PLG aerogels with LOI value up to 43 ± 1.2%, reduced HRR peak value of 25.8 ± 1.0 kW m^{-2} and limited smoke release, and enhanced decomposition temperature up to 550 °C. Therefore, the PLG aerogel with lightweight, robust mechanical, great flame-resistant and super-thermal insulation properties may find broad applications in many civil and military fields.

CRediT authorship contribution statement

Tiantian Xue: Methodology, Investigation, Writing – original draft, preparation. **Wei Fan:** Data curation, Validation, Conceptualization, Writing- Reviewing and Editing, Writing – review & editing. **Xiang Zhang:** Investigation, Data curation. **Xingyu Zhao:** Validation, Formal analysis, Data curation. **Fan Yang:** Formal analysis, Data curation. **Tianxi Liu:** Conceptualization, Methodology, Supervision, Writing-Reviewing and Editing, Writing – review & editing.

Declaration of competing interest

The authors declare that they have no known competing financial interests or personal relationships that could have appeared to influence the work reported in this paper.

Acknowledgements

The authors are grateful for the financial support from the financial support from the Fundamental Research Funds for the Central Universities (2232019A3-03), the National Natural Science Foundation of China (52073053, 21674019), Shanghai Municipal Education Commission (17CG33), Innovation Program of Shanghai Municipal Education Commission (2021-01-07-00-03-E00108), and Science and Technology Commission of Shanghai Municipality (20520741100).

Appendix A. Supplementary data

Supplementary data to this article can be found online at https://doi.org/10.1016/j.compositesb.2021.108963.

References

[1] Sadineni S, Madala S, Boehm R. Passive building energy savings: a review of building envelope components. Renew Sustain Energy Rev 2011;15(8):3617–31.
[2] Li T, Zhu M, Yang Z, Song J, Dai J, Yao Y, et al. Wood composite as an energy efficient building material: guided sunlight transmittance and effective thermal insulation. Adv Energy Mater 2016;6(22):1601122.
[3] Wicklein B, Kocjan A, Salazar-Alvarez G, Carosio F, Camino G, Antonietti M, et al. Thermally insulating and fire-retardant lightweight anisotropic foams based on nanocellulose and graphene oxide. Nat Nanotechnol 2015;10(3):277–83.
[4] Yu Z, Yang N, Zhou L, Ma Z, Zhu Y, Lu Y, et al. Bioinspired polymeric woods. Sci Adv 2018;4(8):7223–33.
[5] Jiang D, Wang Y, Li B, Sun C, Guo Z. Environmentally friendly alternative to polyester polyol by corn straw on preparation of rigid polyurethane composite. Compos Commun 2020;17:109–14.

[6] Du X, Liu H, Mai Y. Ultrafast synthesis of multifunctional N-doped graphene foam in an ethanol flame. ACS Nano 2016;10(1):453–62.
[7] Wang L, Zhang C, Gong W, Ji Y, Qin S, He L. Preparation of microcellular epoxy foams through a limited-foaming process: a contradiction with the time-temperature-transformation cure diagram. Adv Mater 2018;30(3):1703992.
[8] Ruckdeschel P, Philipp A, Retsch M. Understanding thermal insulation in porous, particulate materials. Adv Funct Mater 2017;27(38):1702256.
[9] Yu Z-L, Li G, Fechler N, Yang N, Ma Z, Wang X, et al. Polymerization under hypersaline conditions: a robust route to phenolic polymer-derived carbon aerogels. Angew Chem Int Ed 2016;55(47):14623–7.
[10] Si Y, Yu J, Tang X, Ge J, Ding B. Ultralight nanofibre-assembled cellular aerogels with superelasticity and multifunctionality. Nat Commun 2014;5(1):5802.
[11] Ganonyan N, Benmelech N, Bar G, Gvishi R, Avnir D. Entrapment of enzymes in silica aerogels. Mater Today 2020;33:24–35.
[12] Morris Catherine A, Anderson Michele L, StroudI R, MerzbacherI C, Rolison D. Silica sol as a nanoglue: flexible synthesis of composite aerogels. Science 1999;284:622–4.
[13] Li Y, Liu Y, Liu Y, Lai W, Huang F, Ou A, et al. Ester crosslinking enhanced hydrophilic cellulose nanofibrils aerogel. ACS Sustainable Chem Eng 2018;6(9):11979–88.
[14] Lyu J, Liu Z, Wu X, Li G, Fang D, Zhang X. Nanofibrous kevlar aerogel films and their phase-change composites for highly efficient infrared stealth. ACS Nano 2019;13(2):2236–45.
[15] Zhao N, Yang M, Zhao Q, Gao W, Xie T, Bai H. Superstretchable nacre-mimetic graphene/poly(vinyl alcohol) composite film based on interfacial architectural engineering. ACS Nano 2017;11(5):4777–84.
[16] Song J, Chen C, Yang Z, Kuang Y, Li T, Li Y, et al. Highly compressible, anisotropic aerogel with aligned cellulose nanofibers. ACS Nano 2018;12(1):140–7.
[17] Liu P, Gao H, Chen X, Chen D, Lv J, Han M, et al. In situ one-step construction of monolithic silica aerogel-based composite phase change materials for thermal protection. Compos B Eng 2020;195:108072.
[18] Zhang Q, Wang X, Tao X, Li Z, Li X, Zhang Z. Polyvinyl alcohol composite aerogel with remarkable flame retardancy, chemical durability and self-cleaning property. Compos Commun 2019;15:96–102.
[19] Zhang X, Ni X, Li C, You B, Sun G. Co-gel strategy for preparing hierarchically porous silica/polyimide nanocomposite aerogel with thermal insulation and flame retardancy. J Mater Chem 2020;8(19):9701–12.
[20] Shang K, Liao W, Wang J, Wang Y, Wang Y, Schiraldi D. Nonflammable alginate nanocomposite aerogels prepared by a simple freeze-drying and post-cross-linking method. ACS Appl Mater Interfaces 2016;8(1):643–50.
[21] Wang D, Peng H, Yu B, Zhou K, Pan H, Zhang L, et al. Biomimetic structural cellulose nanofiber aerogels with exceptional mechanical, flame-retardant and thermal-insulating properties. Chem Eng J 2020;389:124449.
[22] Zhu J, Xiong R, Zhao F, Peng T, Hu J, Xie L, et al. Lightweight, high-strength, and anisotropic structure composite aerogel based on hydroxyapatite nanocrystal and chitosan with thermal insulation and flame retardant properties. ACS Sustainable Chem Eng 2020;8(1):71–83.
[23] Fan W, Zhang X, Zhang Y, Zhang Y, Liu T. Lightweight, strong, and super-thermal insulating polyimide composite aerogels under high temperature. Compos Sci Technol 2019;173:47–52.
[24] Wang Y, Cui Y, Shao Z, Gao W, Fan W, Liu T, et al. Multifunctional polyimide aerogel textile inspired by polar bear hair for thermoregulation in extreme environments. Chem Eng J 2020;390:124623.
[25] Wang N, Wang H, Wang Y, Wei Y, Si J, Yuen A, et al. Robust, lightweight, hydrophobic, and fire-retarded polyimide/MXene aerogels for effective oil/water separation. ACS Appl Mater Interfaces 2019;11(43):40512–23.
[26] Liu H, Tian H, Yao Y, Xiang A, Qi H, Wu Q, et al. Polyimide foams with outstanding flame resistance and mechanical properties by the incorporation of noncovalent bond modified graphene oxide. New J Chem 2020;44(28):12068–78.
[27] Laipan M, Yu J, Zhu R, Zhu J, Smith A, He H, et al. Functionalized layered double hydroxides for innovative applications. Mater Horizons 2020;7(3):715–45.
[28] Yao X, Du C, Hua Y, Zhang J, Peng R, Huang Q, et al. Flame-retardant and smoke suppression properties of nano MgAl-LDH coating on bamboo prepared by an in situ reaction. J Nanomater 2019;2019:9067510.
[29] Xu Z, Gao C. Aqueous liquid crystals of graphene oxide. ACS Nano 2011;5(4):2908–15.
[30] Islam A, Mukherjee B, Pandey K, Keshri A. Ultra-fast, chemical-free, mass production of high quality exfoliated graphene. ACS Nano 2021;15(1):1775–84.
[31] Kloprogge J, Wharton D, Hickey L, Frost R. Infrared and Raman study of interlayer anions CO_3^{2-}, NO_3^-, SO_4^{2-} and ClO_4^- in Mg/Al-hydrotalcite. Am Mineral 2002;87(5–6):623–9.
[32] Poli E, Jong KH, Hassanali A. Charge transfer as a ubiquitous mechanism in determining the negative charge at hydrophobic interfaces. Nat Commun 2020;11(1):901.
[33] Li X, Guo M, Bandyopadhyay P, Lan Q, Xie H, Liu G, et al. Two-dimensional materials modified layered double hydroxides: a series of fillers for improving gas barrier and permselectivity of poly(vinyl alcohol). Compos B Eng 2021;207:108568.
[34] Mao J, Zhao C, Li Y, Xiang D, Wang Z. Highly stretchable, self-healing, and strain-sensitive based on double-crosslinked nanocomposite hydrogel. Compos Commun 2020;17:22–7.
[35] Yuan S, Fan W, Wang D, Zhang L, Miao Y, Lai F, et al. 3D printed carbon aerogel microlattices for customizable supercapacitors with high areal capacitance. J Mater Chem 2021;9(1):423–32.
[36] Yu Z, Yang N, Apostolopoulou-Kalkavoura V, Qin B, Ma Z, Xing W, et al. Fire-retardant and thermally insulating phenolic-silica aerogels. Angew Chem Int Ed 2018;57(17):4538–42.
[37] Zhang F, Feng Y, Qin M, Gao L, Li Z, Zhao F, et al. Stress controllability in thermal and electrical conductivity of 3D elastic graphene-crosslinked carbon nanotube sponge/polyimide nanocomposite. Adv Funct Mater 2019;29(25):1901383.
[38] Peng Q, Qin Y, Zhao X, Sun X, Chen Q, Xu F, et al. Superlight, mechanically flexible, thermally superinsulating, and antifrosting anisotropic nanocomposite foam based on hierarchical graphene oxide assembly. ACS Appl Mater Interfaces 2017;9(50):44010–7.
[39] Xu X, Zhang Q, Hao M, Hu Y, Lin Z, Peng L, et al. Double-negative-index ceramic aerogels for thermal superinsulation. Science 2019;363(6428):723–7.
[40] Si Y, Wang X, Dou L, Yu J, Ding B. Ultralight and fire-resistant ceramic nanofibrous aerogels with temperature-invariant superelasticity. Sci Adv 2018;4(4):8925.
[41] Zhang S, Feng J, Feng J, Jiang Y, Li L. Ultra-low shrinkage chitosan aerogels trussed with polyvinyl alcohol. Mater Des 2018;156:398–406.
[42] Yang H, Li Z, Lu B, Gao J, Jin X, Sun G, et al. Reconstruction of inherent graphene oxide liquid crystals for large-scale fabrication of structure-intact graphene aerogel bulk toward practical applications. ACS Nano 2018;12(11):11407–16.
[43] Kobayashi Y, Saito T, Isogai A. Aerogels with 3D ordered nanofiber skeletons of liquid-crystalline nanocellulose derivatives as tough and transparent insulators. Angew Chem Int Ed 2014;53(39):10394–7.
[44] Wang H, Cao M, Zhao H, Liu J, Geng C, Wang Y. Double-cross-linked aerogels towards ultrahigh mechanical properties and thermal insulation at extreme environment. Chem Eng J 2020;399:125698.
[45] Wang T, Long M, Zhao H, Liu B, Shi H, An W, et al. An ultralow-temperature superelastic polymer aerogel with high strength as a great thermal insulator under extreme conditions. J Mater Chem 2020;8(36):18698–706.
[46] Ye D, Wang T, Liao W, Wang H, Zhao H, Wang Y, et al. Ultrahigh-temperature insulating and fire-resistant aerogels from cationic amylopectin and clay via a facile route. ACS Sustainable Chem Eng 2019;7(13):11582–92.
[47] Guo B, Liu Y, Zhang Q, Wang F, Wang Q, Liu Y, et al. Efficient flame-retardant and smoke-suppression properties of Mg-Al-Layered Double-Hydroxide nanostructures on wood substrate. ACS Appl Mater Interfaces 2017;9(27):23039–47.
[48] Fu Z, Wang H, Zhao X, Li X, Gu X, Li Y. Flame-retarding nanoparticles as the compatibilizers for immiscible polymer blends: simultaneously enhanced mechanical performance and flame retardancy. J Mater Chem 2019;7(9):4903–12.
[49] Peng H, Wang D, Zhang L, Li M, Liu M, Wang C, et al. Amorphous cobalt borate nanosheets grown on MoS_2 nanosheet for simultaneously improving the flame retardancy and mechanical properties of polyacrylonitrile composite fiber. Compos B Eng 2020;201:108298.
[50] Zuo L, Fan W, Zhang Y, Zhang L, Gao W, Huang Y, et al. Graphene/montmorillonite hybrid synergistically reinforced polyimide composite aerogels with enhanced flame-retardant performance. Compos Sci Technol 2017;139:57–63.
[51] Peng Y, Cui Y. Advanced textiles for personal thermal management and energy. Joule 2020;4(4):724–42.